

# Out-of-plane spin-to-charge conversion at low temperatures in graphene/MoTe<sub>2</sub> heterostructures

Nerea Ontoso,<sup>1</sup> C.K. Safeer,<sup>1,2</sup> Josep Ingla-Aynés,<sup>1,3</sup> Franz Herling,<sup>1,4</sup> Luis E. Hueso,<sup>1,5</sup> M. Reyes Calvo\*,<sup>6,7</sup> and Fèlix Casanova\*<sup>1,5</sup>

<sup>1</sup>*CIC nanoGUNE BRTA, 20018 Donostia-San Sebastian, Basque Country, Spain*

<sup>2</sup>*Present address: Department of Physics, Clarendon Laboratory, University of Oxford, Oxford, United Kingdom*

<sup>3</sup>*Present address: Kavli Institute of Nanoscience, Delft University of Technology, 2628 CJ Delft, The Netherlands*

<sup>4</sup>*Present address: Catalan Institute of Nanoscience and Nanotechnology (ICN2), 08193 Barcelona, Spain*

<sup>5</sup>*IKERBASQUE, Basque Foundation for Science, 48009 Bilbao, Basque Country, Spain*

<sup>6</sup>*Departamento de Física Aplicada, Universidad de Alicante, 03690 Alicante, Spain*

<sup>7</sup>*Instituto Universitario de Materiales de Alicante (IUMA), Universidad de Alicante, 03690 Alicante, Spain*

(\*Authors to whom correspondence should be addressed: reyes.calvo@ua.es, f.casanova@nanogune.eu)

(Dated: 6 September 2023)

Multi-directional spin-to-charge conversion - in which spin polarizations with different orientations can be converted into a charge current in the same direction - has been demonstrated in low-symmetry materials and interfaces. This is possible because, in these systems, spin to charge conversion can occur in unconventional configurations in which charge current, spin current and polarization do not need to be mutually orthogonal. Here, we explore, in the low temperature regime, the spin-to-charge conversion in heterostructures of graphene with the low-symmetry 1T' phase of MoTe<sub>2</sub>. First, we observe the emergence of charge conversion for out-of-plane spins at temperatures below 100 K. This unconventional component is allowed by the symmetries of both MoTe<sub>2</sub> and graphene and likely arises from spin Hall effect in the spin-orbit proximitized graphene. Moreover, we examine the low-temperature evolution of non-local voltage signals arising from the charge conversion of the two in-plane spin polarizations, which have been previously observed at higher temperature. As a result, we report omni-directional spin-to-charge conversion - for all spin polarization orientations - in graphene/MoTe<sub>2</sub> heterostructures at low temperatures.

Spin-based logic devices offer a promising alternative to the limitations imposed by Joule heating in traditional electronics<sup>1,2</sup>. These spintronic devices rely on the efficient generation, precise control and detection of spin currents, for which materials hosting spin-to-charge conversion (SCC) phenomena provide a platform. SCC occurs in a variety of systems with high spin-orbit interactions; mediated by the spin Hall effect (SHE) in bulk materials<sup>3-5</sup> or the Rashba-Edelstein (REE) effects<sup>6-8</sup> in Rashba interfaces<sup>9</sup> or at the surface states of topological insulators<sup>10,11</sup>.

Spin-orbit-mediated SCC effects were initially investigated in zinc-blende semiconductors and pure metals, such as GaAs<sup>12</sup>, Ta<sup>13</sup> or Pt<sup>14</sup>, all systems with a high degree of crystal symmetry. As a consequence, SCC phenomena have been traditionally expected to appear in configurations where charge current, spin current and spin polarization directions are mutually orthogonal. Nonetheless, these restrictions only hold for materials with high crystal symmetry and are lifted for crystalline phases where certain mirror symmetries are broken<sup>15-18</sup>.

Recent advancements in the preparation of atomically thin layers of van der Waals materials have raised the interest in their spintronic properties. In particular, transition metal dichalcogenides (TMDs) exhibit strong spin-orbit interactions and are good candidates for hosting SCC phenomena. Besides mutually orthogonal conventional SCC, non-orthogonal unconventional SCC configurations have been

recently reported for TMDs with strong spin-orbit coupling and low-symmetry crystal phases<sup>19-24</sup>. Furthermore, TMDs have been integrated in van der Waals heterostructures with graphene, which acts as spin channel due to its long spin diffusion length<sup>25,26</sup>. The combination of SHE and REE effects, enabled by the strong spin-orbit proximity from TMDs to graphene, has led to highly efficient conventional SCC in these heterostructures<sup>27-36</sup>. Additionally, unconventional SCC has been observed in graphene/TMD heterostructures<sup>20,23,37,38</sup>. Symmetry breaking at the van der Waals interface has been proposed to facilitate unusual non-orthogonal SCC in graphene/TMD heterostructures - even for highly symmetric TMD phases<sup>39-44</sup>. As a result, multi- and omni-directional SCC has been already reported for heterostructures of graphene with MoTe<sub>2</sub><sup>20</sup>, WTe<sub>2</sub><sup>37</sup> and NbSe<sub>2</sub><sup>38</sup>, enhancing the efficiency of spin generation and detection and increasing the versatility of graphene/TMD spintronic devices.

Both conventional and unconventional SCC have been observed in the low-crystal-symmetry 1T' phase of MoTe<sub>2</sub> and for graphene/MoTe<sub>2</sub><sup>19-21,33,45</sup>. In Ref.<sup>20</sup>, we reported SCC in a graphene/MoTe<sub>2</sub> heterostructure for the two in-plane spin orientations - one orthogonal and another parallel to the charge current - from 75 K up to room temperature. New SCC processes may emerge at lower temperatures, since conversion in proximitized graphene is enhanced in this regime<sup>27,29</sup>. In this work, we explore SCC in graphene/MoTe<sub>2</sub> lateral spin

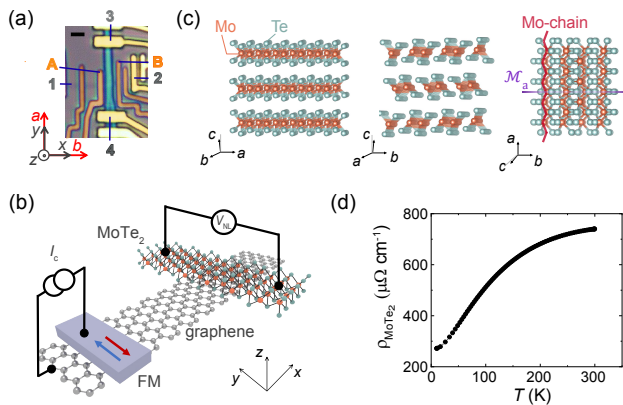


FIG. 1. a) Optical microscope image (scale bar represents  $1 \mu\text{m}$ ) and b) sketch of a graphene/MoTe<sub>2</sub> lateral spin valve device. c) Crystal structure of 1T'-MoTe<sub>2</sub>. Mirror symmetry plane and Mo-chain directions are marked. d) Two-terminal resistance of the MoTe<sub>2</sub> flake as a function of temperature measured using leads 3 and 4 in a.

valve (LSV) devices below 100 K. First, we track the low temperature dependence of both conventional and unconventional SCC for in-plane spin polarization. We find a change of sign of the signal associated to the conventional SCC - allowed by symmetry arguments - that we relate to a change of the relative intensity of two competing effects, namely SHE in MoTe<sub>2</sub> and REE in graphene. More interestingly, we detect the SCC of out-of-plane spin polarization, which increases with lowering temperature and likely arises from SHE in the proximitized graphene. Finally, we summarize all the SCC components observed for graphene/MoTe<sub>2</sub> in our experimental geometry and discuss on their possible origin. Regardless of the conversion mechanisms, we achieve omnidirectional - for all three spin orientations - SCC at low temperature.

LSV devices (Fig. 1a,b) were prepared as described in Refs.<sup>20,21</sup>. A flake of MoTe<sub>2</sub>, with thickness 11 nm, is stacked perpendicularly on top of a graphene channel where magnetic TiO<sub>x</sub>/Co electrodes (labeled as A and B in Fig. 1a) act as spin injectors (FM in Fig. 1b). Needle-like MoTe<sub>2</sub> flakes are typically elongated along the Mo-chain direction (Fig. 1b,c)<sup>20</sup>. Non-magnetic electrodes (Ti/Au) are also deposited both at the ends of the graphene channel and the MoTe<sub>2</sub> flake (labeled as 1-4 in Fig. 1a). Two-terminal resistance measurements as a function of temperature (Fig. 1d) confirm the semimetallic behavior of the MoTe<sub>2</sub> flake, as expected for its thickness<sup>46</sup>. The lack of signatures of structural phase transitions suggests that the MoTe<sub>2</sub> flakes remain in the 1T' phase down to 10 K<sup>19,47</sup>.

To explore SCC phenomena in graphene/MoTe<sub>2</sub> heterostructures, non-local resistance measurements were performed as sketched in Fig. 1b. A current  $I_C = 10 \mu\text{A}$  is applied between the ferromagnetic electrode (FM) and graphene (Fig. 1a,b). The spin accumulation generated at the FM-graphene interface diffuses along the graphene channel, which lies along the  $x$ -direction and can be absorbed at the graphene/MoTe<sub>2</sub> region. The spin current  $j_s$  diffuses along the  $z$ -direction from graphene to MoTe<sub>2</sub> and along the  $x$ -direction to the proximitized graphene. There, if SCC oc-

curs, a non-local voltage  $V_{NL}$  is recorded along the MoTe<sub>2</sub> flake (Fig. 1a,b). It is important to note that, in our experimental geometry (Fig. 1b), only the charge current along the  $y$ -axis direction is detected.  $R_{NL} = V_{NL}/I_C$  is, thus, proportional to the SCC resulting into charge current  $j_c$  along the  $y$ -direction. The orientation of the spin polarization  $s$  reaching the MoTe<sub>2</sub>/graphene region can be controlled along the  $x$ - and  $y$ - directions by switching or pulling the magnetization orientation of the FM injector by an external magnetic field. Additionally, if the field is perpendicular to the spin polarization, spins will precess while diffusing along the graphene channel. Thus, by changing the value of the applied magnetic field along  $x$ -,  $y$ - or  $z$ -directions we can study SCC for the three different spin polarization orientations ( $s^x$ ,  $s^y$  and  $s^z$ ) at the graphene/MoTe<sub>2</sub> heterostructure.

If the magnetic field is applied along the FM in-plane easy axis ( $y$ -direction), a spin current with  $s^y$  will diffuse on the graphene channel without precessing. As  $B_y$  increases, the magnetization of the FM is reversed and a square hysteresis loop appears in Fig. 2a, as the sign of  $R_{NL}$  switches at the coercive field of the FM. This unconventional signal - corresponding to the SCC of  $s^y$  spins - has been already reported at room temperature in Ref.<sup>20</sup>. Conversion of spin polarization into a parallel charge current is forbidden by crystal symmetries both in MoTe<sub>2</sub> (see Supplementary Material) and in graphene. In Ref.<sup>20</sup>, this effect was attributed to symmetry breaking due to strain induced either in the fabrication process or at the van der Waals interface. This signal remains visible down to 10 K, but decreases in amplitude with temperature (Fig. 2a).

Further SCC components can be detected by sweeping the magnetic field in the in-plane hard axis of the FM injector, that is, along the  $x$ -direction ( $B_x$ ). In Fig. 2b,  $R_{NL}$  is measured as a function of  $B_x$  for two different initial states of the FM magnetization. Prior to sweeping  $B_x$ , the FM magnetization is first set along the  $+y$ -direction [ $R_{NL}^\uparrow$ , black curve in Fig. 2b] and then along the  $-y$ -direction [ $R_{NL}^\downarrow$ , red curve in Fig. 2b]. This process is repeated for temperatures from 100 to 10 K. In Ref.<sup>20</sup>, such  $R_{NL}$  measurements were performed from 300 to 100 K (the data at 100 K is the same than in this publication) and the curves were interpreted as the sum of two contributions, one symmetric and another antisymmetric, corresponding, respectively, to the SCC of  $s^x$  and  $s^y$ . This analysis was sufficient to provide an interpretation for the high temperature data. However, Fig. 2b shows how, at very low temperature, the  $R_{NL}$  signal not only changes in size, but it also undergoes significant changes in shape. This suggests the emergence of extra SCC contributions to  $R_{NL}$  that require of a more detailed analysis. To separate the SCC contributions from each spin orientation, it is crucial to consider how they depend on the initial state of the FM magnetization and their parity with respect to the applied magnetic field. Initially, at zero magnetic field, only spins polarized along the FM easy axis ( $s^y$ ) will reach the graphene/MoTe<sub>2</sub> region and contribute to  $R_{NL}$ , with a sign that depends on the initial state of the FM magnetization, either along the  $+y$  or the  $-y$  direction (Fig. 3a). As  $B_x$  increases, the amplitude of the spin  $s^y$  component decays due to spin precession in the  $y$ - $z$ -plane (Fig. 3b) and magne-

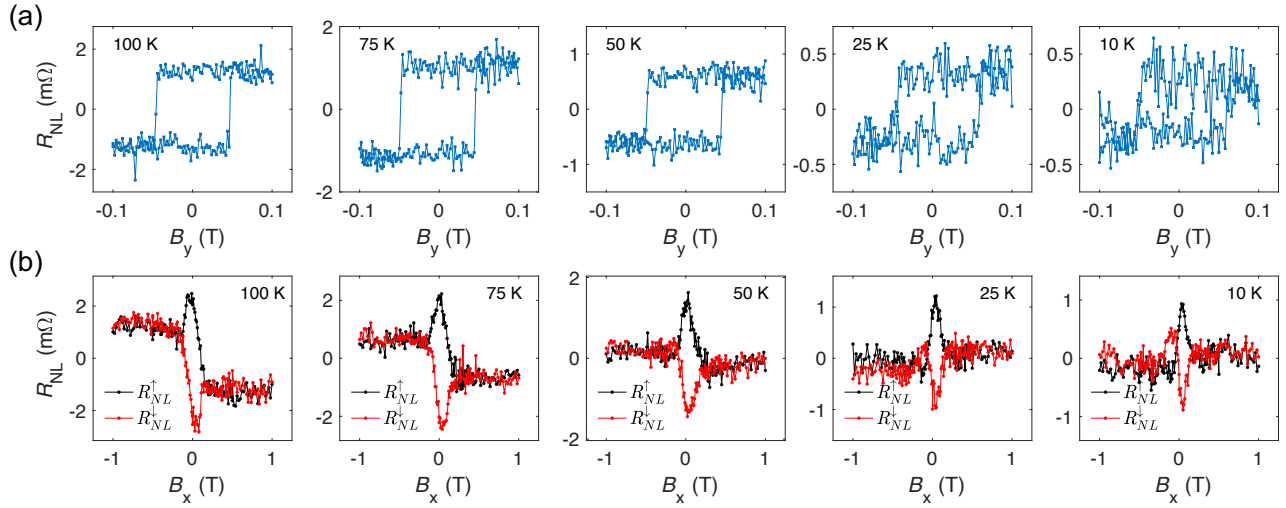


FIG. 2. Non-local resistance  $R_{NL}$  measured with the configuration shown in Fig. 1b, while sweeping the magnetic field in (a) the in-plane FM easy axis  $y$ -direction, and (b) in the in-plane FM hard axis  $x$ -direction. In (b), curves are presented for initial magnetization of the Co electrode saturated along positive (black) and negative (red)  $y$ -direction. Measurements were performed at the temperature indicated in each panel.

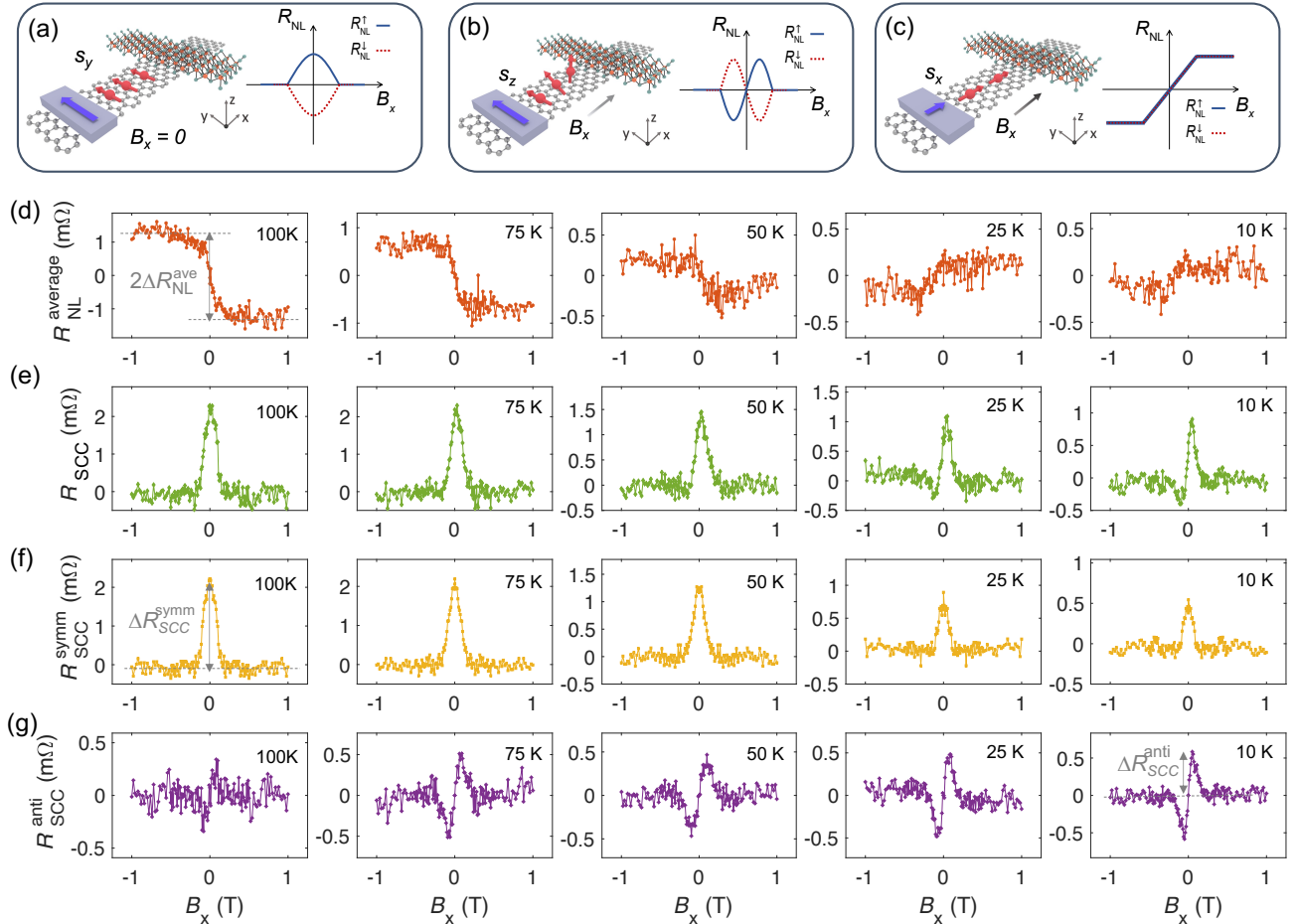


FIG. 3. (a-c) Sketches of the  $R_{NL}$  signal shapes associated to SCC from  $s^y$  (a),  $s^z$  (b) and  $s^x$  (c). (d-g) Analysis of the  $R_{NL}$  versus  $B_x$  curves in Fig. 2b at different temperatures: (d) Average non-local resistance, defined as  $R_{NL}^{average} = (R_{NL}^{\uparrow} + R_{NL}^{\downarrow})/2$ . (e) Spin-to-charge conversion resistance defined as  $R_{SCC} = (R_{NL}^{\uparrow} - R_{NL}^{\downarrow})/2$ . (f) Symmetric component of the  $R_{SCC}$  signal obtained from data in panel e. (g) Anti-symmetric component of the  $R_{SCC}$  signal obtained from data in panel e. All signals are measured at the indicated temperatures.

tization pulling of the injector along the  $x$ -direction (Fig. 3c). As a consequence, the contribution to the  $R_{NL}$  signal coming from SCC of  $s^y$  is symmetric with respect to  $B_x$  and maximum at zero field (Fig. 3a). Also, due to precession in the  $y$ - $z$ -plane field, SCC of  $s^z$  at graphene/MoTe<sub>2</sub> can also be detected in the  $B_x$  sweeps, with its contribution to  $R_{NL}$  being described by an antisymmetric Hanle curve (Fig. 3b). This signal reverses for the two opposite initial states of the injector magnetization (Fig. 3b). Finally, for large values of  $B_x$ , the FM magnetization is aligned along the hard  $x$ -axis and  $s^x$  spins are injected, which do not precess when diffusing along the graphene channel (Fig. 3c).  $R_{NL}$  due to SCC of  $s^x$  is linear at low fields, reaches saturation values at large magnetic field with opposite signs at  $+B_x$  and  $-B_x$  (S-shaped curve), and does not depend on the initial state of the injector magnetization (Fig. 3c).

Because SCC from  $s^x$  is the only contribution to  $R_{NL}$  that does not depend on the initial state of the FM magnetization, it can be extracted by taking the average  $R_{NL}^{average} = (R_{NL}^\uparrow + R_{NL}^\downarrow)/2$  (Fig. 3d). The saturation values of  $R_{NL}^{average}$  as a function of  $B_x$  change sign below 50 K. On the other hand, both SCC contributions from  $s^y$  and  $s^z$  are expected to change sign for opposite initial states of the FM magnetization. Therefore, these contributions are included in  $R_{SCC} = (R_{NL}^\uparrow - R_{NL}^\downarrow)/2$  (Fig. 3e). While the  $s^y$  contribution is symmetric with respect to  $B_x$ , the contribution of  $s^z$  is antisymmetric. This difference allows us to establish an univocal relation between the SCC signal arising from  $s^y$ ,  $R_{SCC}^{symm}$  (Fig. 3f) and the SCC signal from  $s^z$ ,  $R_{SCC}^{anti}$  (Fig. 3g).  $R_{SCC}^{symm}$  shows a maximum at zero field and disappears at the saturation value of  $B_x$  field [Fig. 3f]. This SCC signal is the same one detected in the  $B_y$  sweeps in Fig. 2a and is associated to SCC of  $s^y$  spins in Ref.<sup>20</sup>. More interestingly, at 10 K,  $R_{SCC}^{anti}$  displays a sharp antisymmetric Hanle curve. This signal progressively disappears at higher temperatures, being still visible at 75 K [Fig. 3g] and becoming nearly negligible at 100 K and above (see Supplementary Material and Ref.<sup>20</sup>). These signals evidence the SCC of  $s^z$  spins, which was not observed at higher temperature<sup>20</sup>.

It is important to note that the signals in Fig. 3 are measured as a function of  $B_x$  and, therefore, only  $R_{SCC}^{anti}$  (the  $s^z$  contribution) arises purely from spin precession, confirming its spin origin. In contrast,  $R_{SCC}^{symm}$  and  $R_{NL}^{average}$  are determined not only by precession, but partially or entirely by the pulling of the FM magnetization. Spin precession measurements with applied out-of-plane field ( $B_z$ ) were successfully performed at higher temperatures in Ref.<sup>20</sup>, confirming the spin origin of the SCC signals from  $s^x$  and  $s^y$ , and discarding spurious effects<sup>48</sup>. However, at low temperatures, large backgrounds coming from the magnetoresistance of MoTe<sub>2</sub> and the Hall effect in graphene prevented us from identifying clear Hanle signals. Nevertheless, since the low temperature evolution of the amplitudes of the SCC signals for  $s^x$  and  $s^y$  matches the trend at higher temperatures extracted from Ref.<sup>20</sup> (see Supplementary Material), the spin origin of the  $R_{NL}^{average}$  and  $R_{SCC}^{symm}$  signals can be inferred.

Shunting due to the presence of the MoTe<sub>2</sub> flake prevents us from determining the transport parameters for the proximi-

tized graphene when fitting the data to a Hanle spin precession model. Still, we can extract the amplitude for each SCC component as a function of temperature in the range from 10 K to 100 K, which are presented in Fig. 4a (see Supplementary Material for a comparison with the data at higher temperature from Ref.<sup>20</sup>). The amplitude of  $R_{NL}^{average}$  (coming from SCC of  $s^x$ ) changes sign at low temperature; being negative above 50 K and positive at 25 K and 10 K. At higher temperatures, in Ref.<sup>20</sup>, this contribution was considered to arise from conventional SHE in the bulk of MoTe<sub>2</sub>, with  $s^x$  spins being injected in the  $z$ -direction and resulting in a charge current along  $y$ . In other words,  $R_{NL}^{average}$  may correspond to a conventional configuration of the SHE where where the electric field  $E$ , spin current  $j_s$ , and spin polarization  $s^\alpha$  are mutually orthogonal ( $j_i^\alpha = \sigma_{ij}^\alpha E_j$ , with  $\sigma_{zy}^x$ , see Supplementary Material). However, the conventional REE at the proximitized graphene may also convey SCC in the  $y$ -direction from  $s^x$  (Fig. 4b). Indeed, at low temperatures, the efficiency of proximity-induced REE in graphene, which is expected to be large<sup>29</sup>, could overcome the bulk SHE in MoTe<sub>2</sub> and result in a change of sign of the overall detected signal. Therefore, the sign change of the  $s^x$  signal with lowering T suggests a competition of effects, namely conventional SHE in MoTe<sub>2</sub> and conventional REE in proximitized graphene, with opposite sign in their efficiencies. Nevertheless, since we could not prove the spin origin of the low temperature component, we cannot discard that it might arise from artifacts similar to those observed in Ref.<sup>48</sup>.

Likewise,  $\Delta R_{NL}^{symm}$  (from SCC of  $s^y$ ) decreases with lowering the temperature (Fig. 4a). This can be also seen in Fig. 2a where the amplitude of the  $R_{NL}$  hysteresis loop with  $B_y$  decreases with temperature and becomes barely visible at 10 K. Conversion of  $s^y$  spins into a current in the parallel  $y$ -direction requires the reduction of the system symmetries. This signal can be attributed to an unconventional SHE in MoTe<sub>2</sub> with  $\sigma_{zy}^y$ , only if all mirror symmetries of MoTe<sub>2</sub> are broken, or to an unconventional REE in the proximitized graphene (Fig. 4d). The hypothesis of a REE origin has recently gained force since the shear strain needed to break the MoTe<sub>2</sub> crystal symmetries is expected to be sample-dependent<sup>49</sup>, and this signal has been already observed in several different graphene/MoTe<sub>2</sub> heterostructures<sup>20,21</sup>. Moreover, the misalignment between the mirror planes of graphene and MoTe<sub>2</sub> creates a non-symmetric interface, which enables the unconventional REE mechanism in proximitized graphene<sup>39-44</sup>.

Interestingly,  $\Delta R_{NL}^{anti}$ , observed only at low temperatures and coming from SCC of  $s^z$ , presents its largest value at 10 K and decreases with increasing temperature. Two possible origins can lie behind the conversion of out-of-plane spins: unconventional SHE in MoTe<sub>2</sub>, with  $j_s \parallel s \perp j_c$  and  $\sigma_{zy}^z$  (see Supplementary Material), and conventional SHE in proximitized graphene (with  $j_s \perp s \perp j_c$ ) (Fig. 4c). The non-orthogonal SHE in 1T'-MoTe<sub>2</sub> with spin polarization parallel to the spin current  $\sigma_{zy}^z$ , is allowed by the reduced crystal symmetry and has been reported in Ref.<sup>19</sup> with an efficiency  $\sim 8$  times smaller than the conventional SCC of  $s^x$  ( $\sigma_{zy}^x$ ,  $\Delta R_{NL}^{average}$  in this work). In contrast, SHE in proximitized graphene has been demonstrated to increase significantly with decreasing  $T$ <sup>27,30</sup>. Therefore, even if a non-orthogonal SHE in MoTe<sub>2</sub> cannot

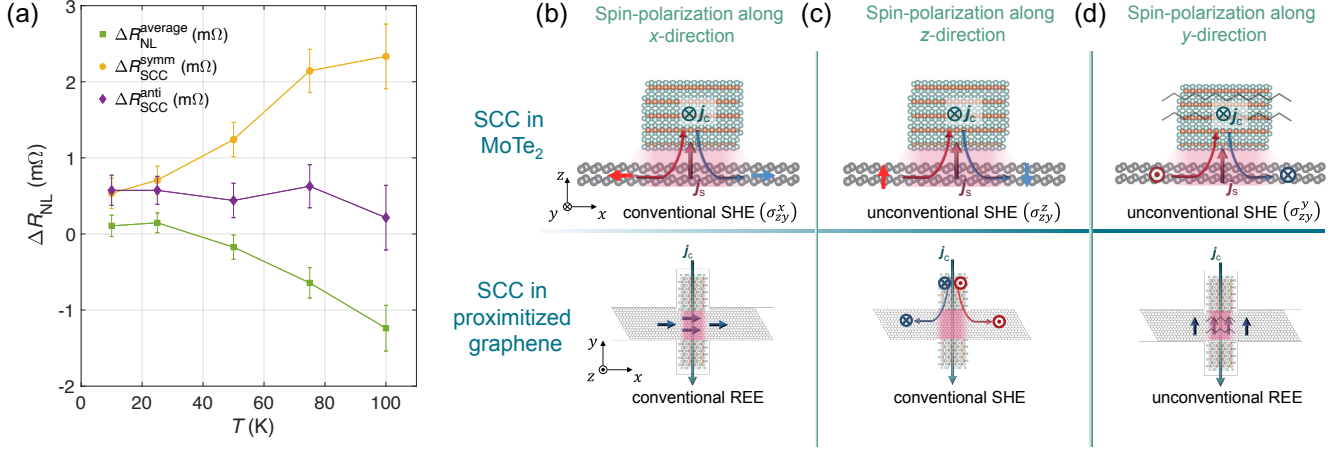


FIG. 4. a) Low-temperature dependence of the amplitude of  $R_{NL}^{average}$  (SCC of  $s^x$ ),  $R_{NL}^{anti}$  (SCC of  $s^z$ ), and  $R_{NL}^{symm}$  (from SCC of  $s^y$ ) extracted from Fig 3. Error bars are calculated from the standard deviation of the signal noise. (b-d) Summary of SCC processes in a graphene/MoTe<sub>2</sub> van der Waals heterostructure that can be detected in our experimental geometry (charge current along the  $y$ -direction). SCC can take place either at the bulk of the MoTe<sub>2</sub> or at the proximitized graphene region, which is represented by a pink halo. (b) SCC of  $s^x$  can occur via the conventional SHE in MoTe<sub>2</sub> if a spin current is injected in the  $z$ -direction ( $\sigma_{zy}^x$ ) or owing to a conventional REE in the proximitized graphene. (c) SCC of  $s^z$  can be attributed to an unconventional, non-orthogonal SHE in MoTe<sub>2</sub> ( $\sigma_{zy}^z$ ) allowed by crystal symmetry but can be also mediated by a conventional SHE in proximitized graphene. (d) SCC of  $s^y$  (parallel to charge current), is allowed only if the mirror symmetry of 1T'-MoTe<sub>2</sub> or the ones of graphene/MoTe<sub>2</sub> interface are broken (represented by a zigzag line), via unconventional, symmetry forbidden, SHE in MoTe<sub>2</sub> ( $\sigma_{zy}^y$ ) or via an unconventional EE in proximitized graphene.

be fully discarded, the rising of  $\Delta R_{NL}^{anti}$  at low temperatures with amplitude larger than  $\Delta R_{NL}^{average}$  points to a conventional SHE in proximitized graphene as the most likely origin for the SCC of  $s^z$  spins. Both the temperature at which the SCC signal from  $s^z$  becomes visible and the temperature at which the SCC signal from  $s^x$  changes sign seem to slightly vary from sample to sample (see Supplementary Material). These facts are compatible with their possible origin from conversion occurring in the proximitized graphene.

In conclusion, we observe omnidirectional SCC in graphene/MoTe<sub>2</sub> van der Waals heterostructures at low temperatures. Firstly, SCC from out-of-plane  $s^z$  spins emerges at low temperatures, likely owing to proximity-induced SHE in graphene. This unconventional component, which is absent at room temperature, is allowed by the symmetries of the system. The SCC signal from  $s^x$ , which reverses sign with  $T$ , is compatible with a competition between mutually orthogonal SHE in MoTe<sub>2</sub> and REE in proximitized graphene, having opposite signs and varying differently in efficiency with temperature. The unconventional SCC from  $s^y$  spins requires mirror symmetries to be broken either at the MoTe<sub>2</sub>, if mediated by unconventional SHE at the bulk of this material, or at the interface between graphene and MoTe<sub>2</sub>, if the origin is unconventional REE in the proximitized graphene. Overall, the results presented in this work, together with those in Refs.<sup>20,21</sup>, make graphene/MoTe<sub>2</sub> a fascinating heterostructure where a plethora of SCC processes arises from different mechanisms. In particular, the crystal structure of MoTe<sub>2</sub> makes this a unique system to further investigate the unconventional components enabled by both the low crystal sym-

metry of the TMD and those appearing in the proximitized graphene interface.

## SUPPLEMENTARY MATERIAL

Supplementary material contains Spin Hall conductivity tensor for 1T'-MoTe<sub>2</sub>, a comparative of the amplitudes of SCC signals at higher temperature, Atomic Force Microscopy characterization of devices and SCC data from a second device.

## ACKNOWLEDGMENTS

This work is supported by the Spanish MICINN under Projects No. PID2021-122511OB-I00, No. MAT2017-88377-C2-2-R, and the Maria de Maeztu Units of Excellence Programme (Grants No. MDM-2016-0618 and No. CEX2020-001038-M); the ‘‘Valleytronics’’ Intel Science Technology Center; the Gipuzkoa Regional Council under Projects No. 2021-CIEN-000037-01; and the European Union H2020 under the Marie Skłodowska-Curie Actions (Grants No. 0766025-QuESTech and No. 794982-2DSTOP). N.O. thanks the Spanish MICINN for support from a Ph.D.fellowship (Grant No. BES-2017-07963). J.I.-A. acknowledges support from the ‘‘Juan de la Cierva-Formación’’ program by the Spanish MICINN (Grant No. FJC2018-038688-I) for a postdoctoral fellowship. R.C. acknowledges funding from Generalitat Valenciana through Grants

No. CIDEAGENT/2018/004, IDIFEDER/2020/005 and IDIFEDER/2021/016.

## DATA AVAILABILITY STATEMENT

The data that support the findings of this study are available from the corresponding author upon reasonable request.

- <sup>1</sup>I. Žutić, J. Fabian, and S. D. Sarma, “Spintronics: Fundamentals and applications,” *Reviews of modern physics* **76**, 323 (2004).
- <sup>2</sup>S. Manipatruni, D. E. Nikonov, C.-C. Lin, T. A. Gosavi, H. Liu, B. Prasad, Y.-L. Huang, E. Bonturim, R. Ramesh, and I. A. Young, “Scalable energy-efficient magnetoelectric spin-orbit logic,” *Nature* **565**, 35 (2019).
- <sup>3</sup>J. Sinova, S. O. Valenzuela, J. Wunderlich, C. Back, and T. Jungwirth, “Spin Hall effects,” *Reviews of modern physics* **87**, 1213 (2015).
- <sup>4</sup>S. O. Valenzuela and M. Tinkham, “Direct electronic measurement of the spin Hall effect,” *Nature* **442**, 176 (2006).
- <sup>5</sup>T. Kimura, Y. Otani, T. Sato, S. Takahashi, and S. Maekawa, “Room-temperature reversible spin Hall effect,” *Physical Review Letters* **98**, 156601 (2007).
- <sup>6</sup>M. I. D’Yakonov and V. I. Perel’, “Spin Orientation of Electrons Associated with the Interband Absorption of Light in Semiconductors,” *Soviet Journal of Experimental and Theoretical Physics* **33**, 1053 (1971).
- <sup>7</sup>M. I. D’Yakonov and V. I. Perel’, “Spin relaxation of conduction electrons in noncentrosymmetric semiconductors,” *Soviet Physics Solid State* **13**, 3581 (1971).
- <sup>8</sup>V. M. Edelstein, “Spin polarization of conduction electrons induced by electric current in two-dimensional asymmetric electron systems,” *Solid State Communications* **73**, 233 (1990).
- <sup>9</sup>J. R. Sánchez, L. Vila, G. Desfonds, S. Gambarelli, J. Attané, J. De Teresa, C. Magén, and A. Fert, “Spin-to-charge conversion using Rashba coupling at the interface between non-magnetic materials,” *Nature communications* **4**, 2944 (2013).
- <sup>10</sup>A. Mellnik, J. Lee, A. Richardella, J. Grab, P. Mintun, M. H. Fischer, A. Vaezi, A. Manchon, E.-A. Kim, N. Samarth, *et al.*, “Spin-transfer torque generated by a topological insulator,” *Nature* **511**, 449 (2014).
- <sup>11</sup>J.-C. Rojas-Sánchez, S. Oyarzún, Y. Fu, A. Marty, C. Vergnaud, S. Gambarelli, L. Vila, M. Jamet, Y. Ohtsubo, A. Taleb-Ibrahimi, *et al.*, “Spin to charge conversion at room temperature by spin pumping into a new type of topological insulator:  $\alpha$ -sn films,” *Physical Review Letters* **116**, 096602 (2016).
- <sup>12</sup>Y. Kato, R. Myers, A. Gossard, and D. Awschalom, “Current-induced spin polarization in strained semiconductors,” *Physical Review Letters* **93**, 176601 (2004).
- <sup>13</sup>L. Liu, C.-F. Pai, Y. Li, H. Tseng, D. Ralph, and R. Buhrman, “Spin-torque switching with the giant spin Hall effect of tantalum,” *Science* **336**, 555 (2012).
- <sup>14</sup>E. Sagasta, Y. Omori, M. Isasa, M. Gradhand, L. E. Hueso, Y. Niimi, Y. Otani, and F. Casanova, “Tuning the spin Hall effect of Pt from the moderately dirty to the superclean regime,” *Physical Review B* **94**, 060412 (2016).
- <sup>15</sup>D. Culcer and R. Winkler, “Generation of spin currents and spin densities in systems with reduced symmetry,” *Physical Review Letters* **99**, 226601 (2007).
- <sup>16</sup>M. Seemann, D. Ködderitzsch, S. Wimmer, and H. Ebert, “Symmetry-imposed shape of linear response tensors,” *Physical Review B* **92**, 155138 (2015).
- <sup>17</sup>Y. Zhang, Q. Xu, K. Koepfernik, R. Rezaev, O. Janson, J. Železný, T. Jungwirth, C. Felser, J. van den Brink, and Y. Sun, “Different types of spin currents in the comprehensive materials database of nonmagnetic spin Hall effect,” *npj Computational Materials* **7**, 1–7 (2021).
- <sup>18</sup>A. Roy, M. H. D. Guimarães, and J. Ślawińska, “Unconventional spin Hall effects in nonmagnetic solids,” *Phys. Rev. Mater.* **6**, 045004 (2022).
- <sup>19</sup>G. M. Stiehl, R. Li, V. Gupta, I. El Baggari, S. Jiang, H. Xie, L. F. Kourkoutis, K. F. Mak, J. Shan, R. A. Buhrman, *et al.*, “Layer-dependent spin-orbit torques generated by the centrosymmetric transition metal dichalcogenide  $\beta$ -MoTe<sub>2</sub>,” *Physical Review B* **100**, 184402 (2019).
- <sup>20</sup>C. K. Safeer, N. Ontoso, J. Ingla-Aynès, F. Herling, V. T. Pham, A. Kurzmann, K. Ensslin, A. Chuvilin, I. Robredo, M. G. Vergniory, F. de Juan, L. E. Hueso, M. R. Calvo, and F. Casanova, “Large multidirectional spin-to-charge conversion in low-symmetry semimetal MoTe<sub>2</sub> at room temperature,” *Nano Letters* **19**, 8758–8766 (2019).
- <sup>21</sup>N. Ontoso, C. K. Safeer, F. Herling, J. Ingla-Aynés, H. Yang, Z. Chi, B. Martín-García, I. Robredo, M. G. Vergniory, F. de Juan, M. Reyes Calvo, L. E. Hueso, and F. Casanova, “Unconventional charge-to-spin conversion in graphene/MoTe<sub>2</sub> van der Waals heterostructures,” *Phys. Rev. Appl.* **19**, 014053 (2023).
- <sup>22</sup>D. MacNeill, G. Stiehl, M. Guimaraes, R. Buhrman, J. Park, and D. Ralph, “Control of spin-orbit torques through crystal symmetry in WTe<sub>2</sub>/ferromagnet bilayers,” *Nature Physics* **13**, 300–305 (2017).
- <sup>23</sup>B. Zhao, B. Karpiak, D. Khokhriakov, A. Johansson, A. M. Hoque, X. Xu, Y. Jiang, I. Mertig, and S. P. Dash, “Unconventional charge-spin conversion in Weyl-semimetal WTe<sub>2</sub>,” *Advanced Materials* **32**, 2000818 (2020).
- <sup>24</sup>I.-H. Kao, R. Muzzio, H. Zhang, M. Zhu, J. Gobbo, S. Yuan, D. Weber, R. Rao, J. Li, J. H. Edgar, *et al.*, “Deterministic switching of a perpendicularly polarized magnet using unconventional spin-orbit torques in WTe<sub>2</sub>,” *Nature Materials* **21**, 1029–1034 (2022).
- <sup>25</sup>N. Tombros, C. Jozsa, M. Popinciuc, H. T. Jonkman, and B. J. van Wees, “Electronic spin transport and spin precession in single graphene layers at room temperature,” *Nature* **448**, 571 (2007).
- <sup>26</sup>J. Ingla-Aynés, M. H. D. Guimarães, R. J. Meijerink, P. J. Zomer, and B. J. van Wees, “24- $\mu$ m spin relaxation length in boron nitride encapsulated bilayer graphene,” *Physical Review B* **92**, 201410 (2015).
- <sup>27</sup>C. Safeer, J. Ingla-Aynés, F. Herling, J. H. Garcia, M. Vila, N. Ontoso, M. R. Calvo, S. Roche, L. E. Hueso, and F. Casanova, “Room-temperature spin Hall effect in graphene/mos2 van der Waals heterostructures,” *Nano Letters* **19**, 107 (2019).
- <sup>28</sup>F. Herling, C. Safeer, J. Ingla-Aynés, N. Ontoso, L. E. Hueso, and F. Casanova, “Gate tunability of highly efficient spin-to-charge conversion by spin Hall effect in graphene proximitized with WSe<sub>2</sub>,” *APL Materials* **8**, 071103 (2020).
- <sup>29</sup>T. S. Ghiasi, A. A. Kaverzin, P. J. Blah, and B. J. van Wees, “Charge-to-spin conversion by the Rashba-Edelstein effect in two-dimensional van der Waals heterostructures up to room temperature,” *Nano Letters* **19**, 5959 (2019).
- <sup>30</sup>L. A. Benitez, W. S. Torres, J. F. Sierra, M. Timmermans, J. H. Garcia, S. Roche, M. V. Costache, and S. O. Valenzuela, “Tunable room-temperature spin galvanic and spin Hall effects in van der Waals heterostructures,” *Nature materials* **19**, 1705 (2020).
- <sup>31</sup>L. Li, J. Zhang, G. Myeong, W. Shin, H. Lim, B. Kim, S. Kim, T. Jin, S. Cavill, B. S. Kim, *et al.*, “Gate-tunable reversible Rashba-Edelstein effect in a few-layer graphene/2H-TaS<sub>2</sub> heterostructure at room temperature,” *ACS nano* **14**, 5251 (2020).
- <sup>32</sup>A. M. Hoque, D. Khokhriakov, B. Karpiak, and S. P. Dash, “Charge-spin conversion in layered semimetal TaTe<sub>2</sub> and spin injection in van der Waals heterostructures,” *Physical Review Research* **2**, 033204 (2020).
- <sup>33</sup>A. M. Hoque, D. Khokhriakov, K. Zollner, B. Zhao, B. Karpiak, J. Fabian, and S. P. Dash, “All-electrical creation and control of spin-galvanic signal in graphene and molybdenum ditelluride heterostructures at room temperature,” *Communications Physics* **4**, 124 (2021).
- <sup>34</sup>B. Zhao, D. Khokhriakov, Y. Zhang, H. Fu, B. Karpiak, A. M. Hoque, X. Xu, Y. Jiang, B. Yan, and S. P. Dash, “Observation of charge to spin conversion in Weyl semimetal WTe<sub>2</sub> at room temperature,” *Physical Review Research* **2**, 013286 (2020).
- <sup>35</sup>J. H. Garcia, M. Vila, A. W. Cummings, and S. Roche, “Spin transport in graphene/transition metal dichalcogenide heterostructures,” *Chemical Society Reviews* **47**, 3359–3379 (2018).
- <sup>36</sup>M. Offidani, M. Milletari, R. Raimondi, and A. Ferreira, “Optimal charge-to-spin conversion in graphene on transition-metal dichalcogenides,” *Physical review letters* **119**, 196801 (2017).
- <sup>37</sup>L. Camosi, J. Světlík, M. V. Costache, W. S. Torres, I. F. Aguirre, V. Marinova, D. Dimitrov, M. Gospodinov, J. F. Sierra, and S. O. Valenzuela, “Resolving spin currents and spin densities generated by charge-spin interconversion in systems with reduced crystal symmetry,” *2D Materials* **9**, 035014 (2022).
- <sup>38</sup>J. Ingla-Aynés, I. Groen, F. Herling, N. Ontoso, C. Safeer, F. de Juan, L. E. Hueso, M. Gobbi, and F. Casanova, “Omnidirectional spin-to-charge con-

- version in graphene/nbse2 van der Waals heterostructures,” *2D Materials* (2022).
- <sup>39</sup>Y. Li and M. Koshino, “Twist-angle dependence of the proximity spin-orbit coupling in graphene on transition-metal dichalcogenides,” *Physical Review B* **99**, 075438 (2019).
- <sup>40</sup>A. David, P. Rakyta, A. Kormányos, and G. Burkard, “Induced spin-orbit coupling in twisted graphene–transition metal dichalcogenide heterobilayers: Twistronics meets spintronics,” *Physical Review B* **100**, 085412 (2019).
- <sup>41</sup>T. Naimer, K. Zollner, M. Gmitra, and J. Fabian, “Twist-angle dependent proximity induced spin-orbit coupling in graphene/transition metal dichalcogenide heterostructures,” *Physical Review B* **104**, 195156 (2021).
- <sup>42</sup>C. G. Péterfalvi, A. David, P. Rakyta, G. Burkard, and A. Kormányos, “Quantum interference tuning of spin-orbit coupling in twisted van der Waals trilayers,” *Physical Review Research* **4**, L022049 (2022).
- <sup>43</sup>A. Veneri, D. T. Perkins, C. G. Péterfalvi, and A. Ferreira, “Twist-angle controlled collinear Edelstein effect in van der Waals heterostructures,” arXiv preprint arXiv:2205.08804 (2022).
- <sup>44</sup>S. Lee, D. de Sousa, Y.-K. Kwon, F. de Juan, Z. Chi, F. Casanova, and T. Low, “Charge-to-spin conversion in twisted graphene/WSe<sub>2</sub> heterostructures,” *Physical Review B* **106**, 165420 (2022).
- <sup>45</sup>P. Song, C.-H. Hsu, G. Vignale, M. Zhao, J. Liu, Y. Deng, W. Fu, Y. Liu, Y. Zhang, H. Lin, *et al.*, “Coexistence of large conventional and planar spin Hall effect with long spin diffusion length in a low-symmetry semimetal at room temperature,” *Nature materials* **19**, 292 (2020).
- <sup>46</sup>P. Song, C. Hsu, M. Zhao, X. Zhao, T.-R. Chang, J. Teng, H. Lin, and K. P. Loh, “Few-layer 1T MoTe<sub>2</sub> as gapless semimetal with thickness dependent carrier transport,” *2D Materials* **5**, 031010 (2018).
- <sup>47</sup>K. Zhang, C. Bao, Q. Gu, X. Ren, H. Zhang, K. Deng, Y. Wu, Y. Li, J. Feng, and S. Zhou, “Raman signatures of inversion symmetry breaking and structural phase transition in type-II Weyl semimetal MoTe<sub>2</sub>,” *Nature communications* **7**, 13552 (2016).
- <sup>48</sup>C. Safeer, F. Herling, W. Y. Choi, N. Ontoso, J. Inglá-Aynés, L. E. Hueso, and F. Casanova, “Reliability of spin-to-charge conversion measurements in graphene-based lateral spin valves,” *2D Materials* **9**, 015024 (2022).
- <sup>49</sup>N. J. Couto, D. Costanzo, S. Engels, D.-K. Ki, K. Watanabe, T. Taniguchi, C. Stampfer, F. Guinea, and A. F. Morpurgo, “Random strain fluctuations as dominant disorder source for high-quality on-substrate graphene devices,” *Physical Review X* **4**, 041019 (2014).